Facility Activity Inference Using Radiation Networks

Camila Ramirez, Nageswara S. V. Rao
Computational Sciences and Engineering Division
Oak Ridge National Laboratory
Oak Ridge, TN 37831
{ramirezca, raons}@ornl.gov

***Abstract*—We consider the problem of inferring the operational status of a reactor facility using measurements from a radiation sensor network deployed around the facility's ventilation off-gas stack. The intensity of stack emissions decays with distance, and the sensor counts or measurements are inherently random with parameters determined by the intensity at the sensor's location. We utilize the measurements to estimate the intensity at the stack, and use it in a one-sided Sequential Probability Ratio Test (SPRT) to infer on/off status of the reactor. We demonstrate the superior performance of this method over conventional majority fusers and individual sensors using (i) test measurements from a network of 21 NaI detectors, and (ii) effluence measurements collected at the stack of a reactor facility. We also analytically establish the superior detection performance of the network over individual sensors with fixed and adaptive thresholds by utilizing the Poisson distribution of the counts. We quantify the performance improvements of the network detection over individual sensors using the packing number of the intensity space.**

***Keywords*-Detection network, sequential probability ratio test, reactor facility, detection, and localization.**

I. Introduction

Inferring the operational status of a reactor facility, using measurements from an independent monitoring system, is critical to the assessment of its compliance to agreements. In particular, such a monitoring system could assist in identifying activities beyond the agreed upon ones, for instance, longer operational periods. In this paper, we consider the problem of inferring the on/off status of a reactor facility by using an on-site network of radiation sensors deployed around the off-gas ventilation stack of the facility, as shown in Figure 1. These sensors measure the emissions from the ventilation stack as counts in keV spectrum, which shows peaks corresponding to radioactive isotopes, for example, 662 keV peak of Cs-137 shown in Figure 2. When the reactor is off, the measurements correspond to background radiation, typically without prominent peaks. When the reactor is on, the measured spectrum reflects emissions from the stack which decay with distance.

The sensors measure intensity levels (at their locations) as gamma spectral counts, but the measurements themselves are inherently random due to the source and background processes [1]. The radiation intensity at the stack is unknown, but the distributions of sensor measurements corresponding to the source and background are closely approximated by the Poisson distribution. The *facility activity inference problem* is to infer the on/off facility status based on measurements collected by sensors at known fixed locations.

This work has been carried out at Oak Ridge National Laboratory managed by UT Battelle, LLC for U.S. Department of Energy under Contract No. DE-AC05-00OR22725.

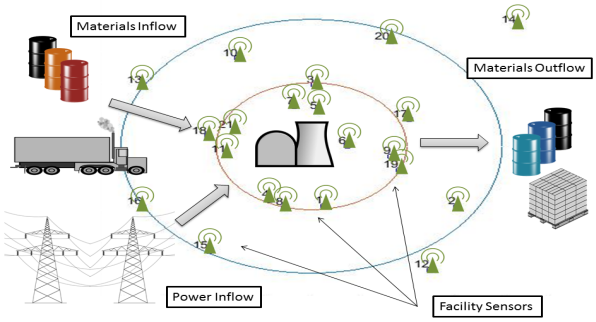

Figure 1. Stack instrumentation of reactor facility.

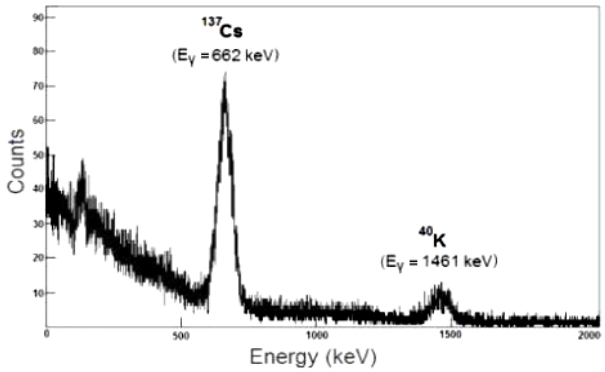

Figure 2. Spectrum of gamma counts.

This problem is a special case of the generic *detection problem* that has been studied extensively using different formulations, for example, a Gaussian source amidst Gaussian background [2] and low-level radiation source amidst comparable background levels [3]–[5]. In particular, a wide range of such detection problems have been solved using Sequential Probability Ratio Tests (SPRTs), including the detection of radiation sources [6]–[8]. For single sensors, typically, the detection problem is solved by choosing appropriate thresholds for SPRT. For a collection of sensors, a simple approach uses the majority of individual decisions. For a network of sensors wherein their locations and measurements can be communicated to a fusion center, better detection performance compared to both methods above can be achieved. In particular, the *localization-based detection method* [9], [10] achieves this by using measurements to estimate source location and

strength, and uses these estimates to adaptively compute SPRT thresholds. In this scenario, both source location and strength are unknown. Our case is somewhat simpler since the location of radiation origin, namely, the stack, is known yet its emission intensity is unknown. However, the intensity measurements are not conducive to inferring the reactor's on/off status by using simple thresholds, thereby requiring methods such as SPRT.

In this paper, we utilize emission measurements to estimate the intensity at the stack, which we then plug into a one-sided SPRT to infer on/off status of the reactor. This method can be viewed as a special case of localization-based detection, wherein the localization is in intensity space compared to intensity-location space in [9]. We demonstrate the practical advantages of our method by using two different testbed measurements. The first datasets come from tests conducted under Domestic Nuclear Detection Office's (DNDO) Intelligence Radiation Sensors Systems (IRSS) program [11], [12]. The second datasets are generated using gas effluence measurements collected on the stack of the High Flux Isotope Reactor (HFIR) in Oak Ridge National Laboratory (ORNL), using a simple quadratic decay model with Poisson distributed measurements [1]. In both cases, we show the superior performance of our method over conventional majority fusers and individual sensors, in terms of false alarm and detection probabilities.

We also analytically establish the superior detection performance of our network method over individual sensors with fixed and adaptive thresholds, by utilizing the Poisson distribution of the counts. Additionally, we quantify the performance improvements of the network detection over individual sensors using the packing number of the intensity state-space. Similar results have been derived for the more general source detection problems in [9], and here we sharpen those results and simplify the proof for our one-dimensional problem.

The rest of the paper is organized as follows. We formulate the facility activity inference problem in Section II. In Sections III and IV, respectively, we discuss experimental results and performance comparisons based on IRSS and HFIR datasets. We present analytical results which establish performance bounds on detection and false alarm rates of the network detection method relative to those of the other methods, in Section V.

II. Detection Problem

We consider a two-dimensional monitoring area $\mathcal{M} \subseteq \Re^2$, such as a $[0, D] \times [0, D]$-grid, with $D < \infty$, for detecting the presence of unknown intensity $A_S \in \mathcal{A}$, with $\mathcal{A} := (0, A_{Max}]$ and $A_{Max} < \infty$, at the stack S located at $(x_S, y_S) \in \mathcal{M}$. There is a background process of noise characterized by intensity parameter $B \in \mathcal{B}$, with $\mathcal{B} := (0, B_{Max}]$ and $B_{Max} < \infty$, parameterized by P_B.

In order to monitor $\mathcal{M}$, a network of N sensors are deployed, with sensor i located at $M_i := (x_i, y_i) \in \Re^2$, for $i = 1, 2, \ldots, N$. Given a point $P := (x, y) \in \Re^2$, we have the distance $d(P, M_i) = \sqrt{(x - x_i)^2 + (y - y_i)^2 + h^2}$, for $i \in \{1, \cdots, N\}$ and where h is the height of the stack. The measurements at sensor i are characterized as follows:

(a) *Background measurements:* When the facility is off, the "background" measurements at sensor i are distributed according to P_{B_i}, with $B_i = B$.

(b) *Source measurements:* When the facility is on, the intensity within a spectral band at the sensor's location (x_i, y_i) is a function of A_S and $d(S, M_i) = d((x_S, y_S), M_i)$, that is $A_i = \frac{A_S}{d(S,M_i)^2}$. We represent this dependence explicitly as a function $A_i = F_S(A_S, x_S, y_S, x_i, y_i)$. The measurements of A_i collected by sensor i are distributed according to $P_{A_i+B_i}$.

The underlying measurement distributions P_{B_i} and $P_{A_i+B_i}$ are Poisson processes with parameters B_i and $A_i + B_i$, respectively [1], [8], [13].

Let $\{m_{i,1}, m_{i,2}, \ldots, m_{i,n_i}\}$ be the sequence of measurements collected by sensor i during the time window of interest. The radiation count $m_{i,j}$ observed at the location M_i at time j is a Poisson-distributed random variable with parameter $\lambda = B_i$ if the reactor is off, or with parameter $\lambda = A_i + B_i$ if the reactor is on, which is approximated as a point radiation source [1]. The probability of the measurement $m_{i,j}$ at sensor i is given by its likelihood function $L(m_{i,j}) = \frac{\lambda^{m_{i,j}} e^{-\lambda}}{m_{i,j}!}$, where $\lambda \in \{A_i + B_i, B_i\}$.

The performance of a detection method is characterized by its (i) *false alarm probability* $P_{0,1}$, corresponding to the probability of declaring the presence of a source when none exists, that is, declaring that reactor is on while it is off, and (ii) *missed detection probability* $P_{1,0}$, corresponding to the probability of declaring the presence of only the background process when a source is present, that is, failing to detect that reactor is on. The *detection probability* is given by $P_{1,1} = 1 - P_{1,0}$, which is the probability of declaring a source when one is present in the monitoring area.

A. SPRT Detection

The SPRT utilizes likelihood functions to decide between the hypotheses H_{A+B} and H_B corresponding to a source amidst the background and the background only, respectively. Let $L(m_1, m_2, \ldots, m_n | H_\lambda)$, for $\lambda \in \{A + B, B\}$, denote the likelihood of the measurements $m_1, m_2, \ldots, m_n$ under the hypothesis H_λ. The ratio of likelihoods:

$$\mathcal{L}_{A,B,n} = \frac{L(m_1, m_2, \ldots, m_n | H_{A+B})}{L(m_1, m_2, \ldots, m_n | H_B)}$$

is used by SPRT for detecting the source with false positive and missed detection probabilities $P_{0,1}$ and $P_{1,0}$, respectively, as follows [14]:

(i) If $\mathcal{L}_{A,B,n} < \frac{P_{0,1}}{1-P_{1,0}}$, declare the background H_B;

(ii) Else if $\mathcal{L}_{A,B,n} > \frac{1-P_{0,1}}{P_{1,0}}$, declare a source H_{A+B};

(iii) Otherwise, declare the measurements to be insufficient for making a decision.

This SPRT is compactly denoted as:

$$\frac{P_{0,1}}{1 - P_{1,0}} \leq \mathcal{L}_{A,B,n} \leq \frac{1 - P_{0,1}}{P_{1,0}}.$$

We consider two different applications of SPRT for the detection problem. First, when measurements are collected from a single sensor, $A \in \Re$ and $B \in \Re$ correspond to the source and background intensities, respectively, at the location

M_i. Second, when measurements are collected from sensors at N different locations, we use vectors $\mathbf{A} \in \Re^N$ and $\mathbf{B} \in \Re^N$ to denote the source and background intensities, respectively, at all these locations. We now express this test in terms of measurements only. For a single detector, the likelihood function is:

$$L(m_{i,1}, m_{i,2}, \ldots, m_{i,n_i}|H_\lambda) = \prod_{j=1}^{n_i} \frac{\lambda^{m_{i,j}} e^{-\lambda}}{m_{i,j}!},$$

where $\lambda \in \{B_i, A_i + B_i\}$. The SPRT for detection can be expressed in terms of the sum of measurements as [15]:

$$\frac{\ln\left[\frac{P_{0,1}}{1-P_{1,0}}\right] + n_i A_i}{\ln\left[\frac{A_i+B_i}{B_i}\right]} \leq \sum_{j=1}^{n} m_{i,j} \leq \frac{\ln\left[\frac{1-P_{0,1}}{P_{1,0}}\right] + n_i A_i}{\ln\left[\frac{A_i+B_i}{B_i}\right]}.$$

This is an example of the separable test defined in [9] to be expressed as:

$$\begin{aligned} F_L(P_{0,1}, P_{1,0}, A, B, n) &< \sum_{i=1}^{n} m_i \\ &< F_U(P_{0,1}, P_{1,0}, A, B, n), \end{aligned}$$

for suitable lower and upper threshold functions, $F_L(\cdot)$ and $F_U(\cdot)$ respectively, where A and B are the source and background intensity levels. Furthermore, the sensor measurements are statistically independent not only across time but also across sensors, and hence satisfy the following conditions:

$$L_i(m_{i,1}, m_{i,2}, \ldots, m_{i,n_i}|H_\lambda) = \prod_{j=1}^{n_i} L_i(m_{i,j})$$

$$L_\pi(m_{1,j}, m_{2,j}, \ldots, m_{N,j}|H_\lambda) = \prod_{i=1}^{N} L_i(m_{i,j}),$$

where $L_i(m_{i,j})$ is the probability of measurement $m_{i,j}$ at sensor i and $\lambda \in \{\mathbf{A} + \mathbf{B}, \mathbf{B}\}$. Therefore, when measurements are collected from sensors at N different locations, the SPRT can be expressed as:

$$\ln\left[\frac{P_{0,1}}{1-P_{1,0}}\right] \leq \sum_{i=1}^{N} \ln\left[\frac{A_i+B_i}{B_i}\right] m_{i,j} - \sum_{i=1}^{N} A_i \leq \ln\left[\frac{1-P_{0,1}}{P_{1,0}}\right].$$

These properties are satisfied in the case of point radiation sources, which show that the corresponding weighted SPRT is separable and can be expressed in a more general form:

$$\begin{aligned} F_L(P_{0,1}, P_{1,0}, \mathbf{A}, \mathbf{B}, N) &< \sum_{i=1}^{N} w_i m_i \\ &< F_U(P_{0,1}, P_{1,0}, \mathbf{A}, \mathbf{B}, N), \end{aligned}$$

for suitable lower and upper threshold functions, $F_L(\cdot)$ and $F_U(\cdot)$ respectively, and w_i is the weight assigned to measurement m_i.

The upper and lower threshold functions $F_U(\cdot)$ and $F_L(\cdot)$ depend on the unknown source intensity, and hence cannot be directly computed. In practice, threshold values $\tau_L = F_L(\cdot)$ and $\tau_U = F_U(\cdot)$ are often chosen based on domain-specific considerations and the target false alarm rate $P_{0,1}$ and missed detection rate $P_{1,0}$.

B. Stack Intensity Estimation

Using n N-tuple source network measurements, of the form $(m^S_{1,j}, \cdots, m^S_{N,j})$ for $j = 1, \cdots, n$, we compute the estimate $\hat{A}_S$ of A_S as:

$$\hat{A}_S = \frac{1}{nN} \sum_{i=1}^{N} d_i^2 \left(\sum_{j=1}^{n} m^S_{i,j} \right).$$

Similarly, we also estimate the background intensity as:

$$\hat{B} = \frac{1}{nN} \sum_{i=1}^{N} \left(\sum_{j=1}^{n} m^B_{i,j} \right).$$

The source estimate is δ-*robust* in that there exists $\delta(\epsilon, n, N) \in [0, 1]$, which is a non-decreasing function of precision ϵ, such that:

$$P\left\{ \hat{A}_S \in \mathfrak{A}_{S,\epsilon} \right\} > \delta(\epsilon, n, N),$$

where $\mathfrak{A}_{S,\epsilon} = \{a \in \mathcal{A} | d(a, A_S) < \epsilon\}$ is called the ϵ-*precision* region. A localization method is *monotone robust* if $\delta(\epsilon, n, N)$ is a non-decreasing function on the number of measurements n and sensors N. Monotone robustness ensures that the estimate is within an ϵ-precision region around the source intensity A_S with probability δ, which improves as more measurements and sensors are utilized. This condition is a reasonable requirement in general, and in our particular case, it is satisfied by a version of Hoeffding's inequality (e.g. in [16]):

$$P(|\hat{A}_S - A_S| < \epsilon) \geq 1 - e^{\frac{-2nN\epsilon^2}{A_{Max}}},$$

since the measurements are statistically independent in time and across the sensors.

III. IRSS Experimental Results

In this section, we experimentally address the facility activity inference problem posed in Section II, that is, infer the on/off status of a reactor facility by using an on-site network of radiation sensors deployed around the off-gas ventilation stack, by making use of IRSS datasets. We treat the stack as 2-dimensional, positioned at the IRSS datasets source location, with a network of 21 NaI detectors placed around it. The role of the stack is emulated by a low-radiation source and the NaI sensors play the role of network deployment. We first describe the datasets used in our testing, then consider experimental intensity-estimation SPRTs, and lastly make performance comparisons in order to assess network methods superior detection.

A. IRSS Datasets

DNDO IRSS supported the development of networks of commercial-off-the-shelf radiation counters for detecting, localizing, and identifying low-level radiation sources. Under this program, a series of indoor and outdoor tests were conducted with multiple source strengths and types, different background profiles, and various types of source and detector movements. Following the tests, network algorithms were replayed in various re-constructed scenarios using sub-networks. Together, these measurements and algorithm traces provide a rich collection of highly valuable datasets for testing the current and next generation radiation network algorithms, including the ones (to be) developed by broader R&D communities such as distributed detection, information fusion, and sensor networks.

The first batch of canonical datasets for public use includes measurements from ten indoor and two outdoor tests which

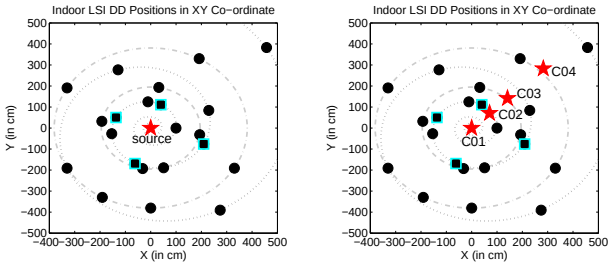

(a) Stationary source. (b) Off-set source.

Figure 3. Indoor test configurations.

represent increasingly challenging baseline scenarios for robustly testing radiation network algorithms. The indoor tests were performed in the Low Scatter Irradiator (LSI) facility at the Savannah River National Laboratory (SRNL). There were 17 NaI 2"×2" and 4 other stationary detectors laid out in a spiral and two concentric circles around the center of the testing facility, as shown in Figure 3(a). Radiation counts collected by each detector were mapped into 21 spectral bins. Several experiments were conducted both with stationary and moving sources of various strengths and types.

Our tests make use of the following datasets:

1) Background Measurements: Background counts are collected at all detectors with no source present to characterize the background radiation levels of LSI.

2) Cs-137 Source at Center: The detector counts for a stationary 35μCi Cs-137 source are collected by placing the source at the center of the detector field.

3) Co-57 Source at Center: Similar to Cs-137 test, the detector counts for a stationary 45μCi Co-57 source located at the center are also measured.

4) Source Off-Set from Center: The effects of asymmetrical configurations of the source and detectors are captured by placing a stationary 7.6μCi Cs-137 source at 0m (Cs-137_1), 1m (Cs-137_2), 2m (Cs-137_3), and 4m (Cs-137_4) diagonally offset from the center towards the northeast area of detector field, see Figure 3(b).

B. Experimental SPRTs

In order to assess the effectiveness of detection using intensity estimates, we device three left-handed intensity-estimation SPRTs (LH-IE SPRT) and test them on six different pairings of IRSS datasets. This means that for the background measurements along with each of the five different source datasets described above, we perform single sensors, simple majority, and sensor fusion LH-IE SPRTs. Each dataset is composed of 9 runs with 120 measurements each. We divide the set of runs in half to allocate data for both training and testing. Furthermore, we set a *window size* for all runs, for example, a window of size $w = 5$ produces 116 *window measurements* for each run. In implementing our three types of LH-IE SPRTs, we use different window sizes and resulting window measurements.

Moreover, for all 21 sensors, we compute the distance between sensor i and source S; discarding sensors whose distance to the source is greater than the maximum distance plus the mean distance divided by some factor, that is if $d(S, M_i) > \frac{d(S,M_i)_{Max}+\overline{d(S,M_i)}}{4.5}$. Using training data, we estimate the source intensity as:

$$\hat{A}_S = \frac{1}{nKN}\sum_{i=1}^{N} d_i^2 \left(\sum_{k=1}^{K}\sum_{j=1}^{n} m_{i,k,j}^{S_w}\right)$$

with $m_{i,k,j}^{S_w}$ a source-present window measurement, $K = 4$ and $n = 121 - w$. Similarly, we estimate the background intensity as:

$$\hat{B} = \frac{1}{nKN}\sum_{i=1}^{N} \left(\sum_{k=1}^{K}\sum_{j=1}^{n} m_{i,k,j}^{B_w}\right).$$

We also compute both intensities at sensor locations, that is $\hat{A}_i = \frac{\hat{A}_S}{d(S,M_i)^2}$ and $\hat{B}_i = \hat{B}$ for $i = 1, \cdots, N$. We set the false detection to $P_{0,1} = 0.1$ and true detection to $P_{1,1} = 0.9$. Lastly, we compute the SPRT weights, $w_i = \ln \frac{\hat{A}_i+\hat{B}_i}{\hat{B}_i}$ for each sensor i.

For single sensors and simple majority tests, the adaptive thresholds are of the form:

$$\tau_{L_i} = \ln \frac{P_{0,1}}{1 - P_{1,0}} + \hat{A}_i,$$

whereas in the sensors fusion test:

$$\tau_L = \ln \frac{P_{0,1}}{1 - P_{1,0}} + \sum_{i=1}^{N} \hat{A}_i.$$

These LH-IE SPRTs are performed multiple times on each combination of datasets (as specified above) using window sizes starting at $w = 1$ and increasing by a factor of 5 at every iteration ending with $w = 56$.

C. Performance Comparison

We estimate the false alarm and detection rates of various LH-IE SPRT classifiers, i.e. single sensors, simple majority, and sensors network. The results are summarized in ROC curves as shown in Figure 4 to Figure 9, wherein the false alarm and detection rates are on Y axes and the window size on the X axes. In general for a classifier, lowering of the threshold parameter leads to higher detection rate but also increases the false alarm rate. The desired performance of a classifier is a high detection rate at a low false alarm rate, as indicated by the sensors network LH-IE SPRT when applied to all six pairs of datasets.

These ROC curves illustrate how even after eliminating sensors which are far away from the source, not all of the remaining detectors perform well under the single sensors test. This is particularly evident in the datasets containing Cs-137 at low intensity 7.6μCi, see Figure 6 to Figure 9. The simple majority test seems to perform reasonably well, yet it is not completely effective when dealing with a low intensity source or when the source is farther away from the bulk of the sensors, as shown in Figure 6 and Figure 9, respectively. On the other hand, the LH-IE SPRT fuser performed consistently well, achieving optimal detection within a few iterations of window size increase.

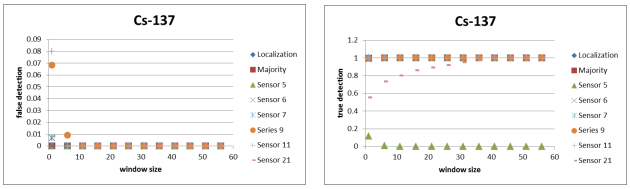

(a) False detection. (b) True detection.

Figure 4. Cs-137 Roc Curves.

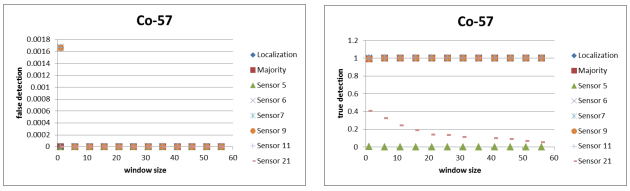

(a) False detection. (b) True detection.

Figure 5. Co-57 Roc Curves.

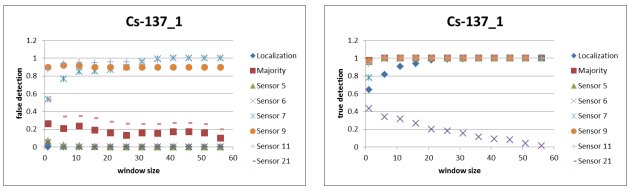

(a) False detection. (b) True detection.

Figure 6. Cs-137 1 Roc Curves.

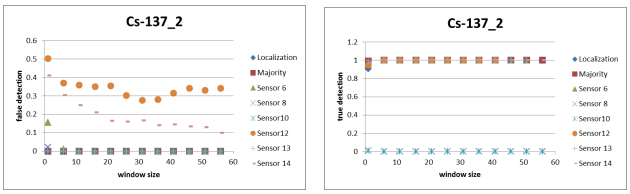

(a) False detection. (b) True detection.

Figure 7. Cs-137 2 Roc Curves.

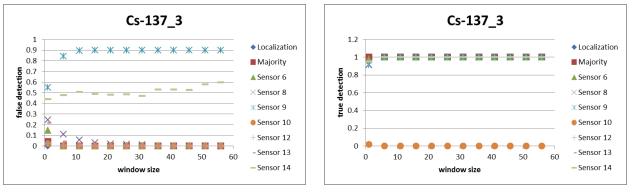

(a) False detection. (b) True detection.

Figure 8. Cs-137 3 Roc Curves.

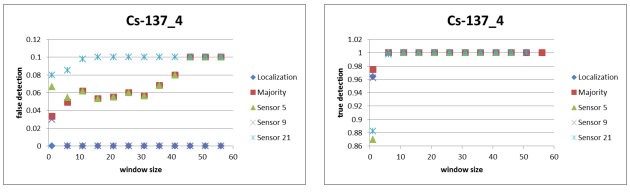

(a) False detection. (b) True detection.

Figure 9. Cs-137 4 Roc Curves.

IV. HFIR Experimental Results

Our second testbed consists of artificially generated datasets developed from effluence measurements of three gases, namely, Ar-41, Cs-138, and Xe-138, collected on the stack of HFIR in ORNL. We again test the sensors network, single detectors, and simple majority LH-IE SPRTs on each of the datasets. We conclude the section with SPRTs performance comparisons for each isotope.

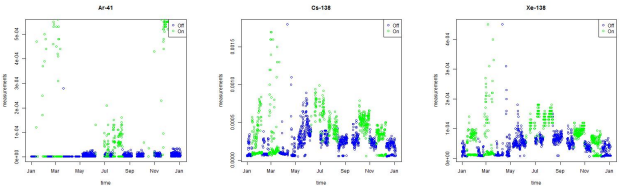

(a) Ar-41. (b) Cs-138. (c) Xe-138.

Figure 10. On/Off Effluence Measurements.

A. HFIR Datasets And Experimental SPRTs

Effluence measurements of Ar-41, Cs-138, and Xe-138 gases are collected on the stack of HFIR in ORNL. These gases are continuously monitored using a feeding tube in the stack, and the measurements are provided and statistically analyzed every four hours. The stack itself is shared by another reprocessing facility at ORNL, which complicates the on/off classification task for HFIR. The Figures 10(a), 10(b), and 10(c) show scatter plots of the ground truth data corresponding to Ar-41, Cs-138, and Xe-138, for on/off periods of HFIR from January 2015 to January 2016.

For each of these gases, we use its effluent measurements to estimate the intensity of radiation at the stack for both on/off periods, that is, $\hat{A}_S = \bar{m}_i^{On}$ and $\hat{B} = \bar{m}_i^{Off}$, where $\bar{m}_i$ is the mean measurement and $i \in \{Ar-41, Cs-138, Xe-138\}$. We assume that the stack S is located in the center of a detection field and generate 21 random positions, M_j for $j \in \{1, \cdots, 21\}$, around S with assigned intensities $\hat{A}_j = \frac{\hat{A}_S}{d(S,M_j)^2}$ and $\hat{B}_j = \frac{\hat{B}}{d(S,M_j)^2}$. As in the previous section, we discard positions whose distance from the stack are greater than a fixed radius. Using the intensities corresponding to the remaining locations, we create Poisson distributions and artificially generate datasets for both on/off activity periods, that is, $\{m_{j,k}^{On}\}_{k=1}^m \sim Pois(c\hat{A}_j)$ and $\{m_{j,k}^{Off}\}_{k=1}^m \sim Pois(c\hat{B}_j)$ for $j \in \{i, \cdots, N\}$ and $c \in \mathfrak{N}$. We again define window sizes, detection rates, and SPRT weights as in Section III, the adaptive thresholds are defined as:

$$\tau_{L_j} = \ln \frac{P_{0,1}}{1-P_{1,0}} + c\hat{A}_j, \quad \tau_L = \ln \frac{P_{0,1}}{1-P_{1,0}} + \sum_{j=1}^{N} c\hat{A}_j.$$

We perform single sensors, simple majority, and sensor network LH-IE SPRTs multiple times for each gas type, using window sizes $w \in \{1, \cdots, n+5, \cdots, 56\}$.

B. Performance Comparison

We estimate the false alarm and detection rates of single sensors, simple majority, and sensors network LH-IE SPRT classifiers using artificially generated datasets. The results are summarized in ROC curves as shown in Figure 11 to Figure

13. These ROC curves illustrate how even after eliminating sensors which are far away from the stack, not all of the remaining detectors perform well under the single sensors test. This is particularly evident in the datasets corresponding to a source of either Cs-138 or Xe-138, see Figure 12(a) and 13(a). The simple majority test as well as the network SPRT, seem to perform well in the case of Ar-41. Yet for Cs-138 and Xe-138. simple majority fails to detect almost all measurements coming from off-periods, as shown in Figure 12(a) and Figure 13(a). We conclude that SPRT fuser is consistently better and hypothesize an increase in window size will further lower the false alarm detection rate of Xe-138.

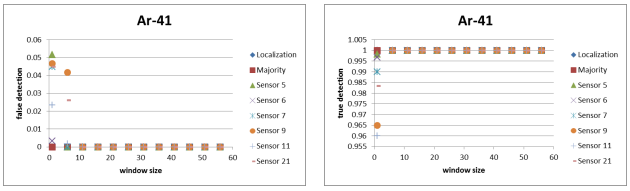

(a) False detection. (b) True detection.

Figure 11. Ar-41 Roc Curves.

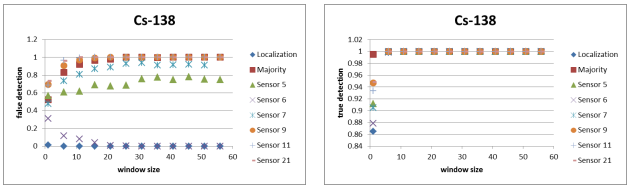

(a) False detection. (b) True detection.

Figure 12. Cs-138 Roc Curves.

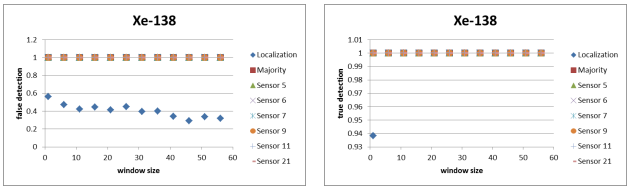

(a) False detection. (b) True detection.

Figure 13. Xe-138 Roc Curves.

V. Detection Based on Intensity Estimation

Recall the stack intensity estimates $\hat{A}_S$ and $\hat{B}$ defined in Section II. In this section, we use those estimates to derive sharpened versions of the SPRTs. We first consider sensor measurements collected at a single location, and then consider measurements from sensors at different locations in the network.

A. Single Location Measurements

The source and background intensity estimates $\hat{A}_S$ and $\hat{B}$ are substituted into the threshold function of the SPRT, based on $n_\alpha := n$ measurements $\{m_i | i = 1, 2, \ldots, n\}$, for $\alpha = 1, 2, \ldots, N$, as follows:

$$F_L(P_{0,1}, P_{1,0}, \hat{A}_\alpha, \hat{B}, n) < \sum_{i=1}^{n} m_i < F_U(P_{0,1}, P_{1,0}, \hat{A}_\alpha, \hat{B}, n),$$

where $\hat{A}_\alpha = F_S(\hat{A}_S, x_S, y_S, x_\alpha, y_\alpha)$. We denote this *location-based* SPRT by $\mathcal{L}_{\alpha;\hat{S}}$.

For SPRT $\mathcal{L}$, we denote the detection and false alarm probabilities by $\mathcal{E}_D(\mathcal{L})$ and $\mathcal{E}_F(\mathcal{L})$, respectively. Let $\mathcal{A} = (0, A_{Max}] \subseteq \Re$ denote the set of all possible source intensities. An open *cell* with center $a_k \in \mathcal{A}$ and radius ρ_A is defined as:

$$\mathcal{C}_k = \{a \in \mathcal{A} | d(a, a_k) < \rho_A\},$$

where $d(a_1, a_2) = |a_1 - a_2|$. We define $\mathcal{C}_0$ to be the cell located at $a = \rho_A$.

Definition 5.1: A *ρ_A-packing* of the state space $\boldsymbol{\mathcal{A}} := \mathcal{A}$ corresponds to disjoint cells with *cell centers* at a_k, $k = 1, 2, \ldots, K$ and of radius ρ_A all contained inside the state space $\boldsymbol{\mathcal{A}}$. We define such a packing to be *translation invariant* if all the cells are still inside $\boldsymbol{\mathcal{A}}$ when their centers are translated as $a + a_k$, for all $a \leq \rho_A$. The *state packing number* $\boldsymbol{\mathcal{M}}(\boldsymbol{\mathcal{A}}, \rho_A)$ denotes the maximum size of a translation-invariant ρ_A-packing of the state space $\boldsymbol{\mathcal{A}}$.

Note this number will be m or $m-1$ for $A_{Max} = 2\rho_A m + r$, depending on the value $0 \leq r < 2\rho_A$.

We define the *upper-threshold set* $\boldsymbol{\mathcal{S}}_{\alpha,\tau_U}$ and *lower-threshold set* $\boldsymbol{\mathcal{S}}_{\alpha,\tau_L}$ to represent all the possible source intensities and SPRT bound functions corresponding to the thresholds of $\mathcal{L}_{\alpha;[\tau_L,\tau_U]}$, for $\alpha = 1, 2, \ldots, N$, as follows:

$$\boldsymbol{\mathcal{S}}_{\alpha;\tau_L} = \{A_S \in \boldsymbol{\mathcal{A}} \mid \tau_L = F_L(P_{0,1}, P_{1,0}, \hat{A}_\alpha, \hat{B}, n_\alpha); \hat{A}_\alpha \geq F_S(A_S, x_S, y_S)\} \quad \text{and}$$

$$\boldsymbol{\mathcal{S}}_{\alpha;\tau_U} = \{A_S \in \boldsymbol{\mathcal{A}} \mid \tau_U = F_U(P_{0,1}, P_{1,0}, \hat{A}_\alpha, \hat{B}, n_\alpha); \hat{A}_\alpha \geq F_S(A_S, x_S, y_S)\}.$$

For sensor measurements collected at a single location, the following result generalizes Theorem 3.1 of [17]. It characterizes the performance improvements of $\mathcal{L}_{\alpha;\hat{S}}$ over its thresholded version $\mathcal{L}_{\alpha;[\tau_L,\tau_U]}$, as a function of the packing number $\boldsymbol{\mathcal{M}}(\cdot)$ and the quality of localization given by $\delta(\cdot)$.

Theorem 5.1: Consider the detection of a source using separable SPRTs. For $\alpha = 1, 2, \ldots, N$ and sufficiently large n_α take SPRT $\mathcal{L}_{\alpha;\hat{S}}$, based on a monotone δ-robust localization method and any threshold-based SPRT $\mathcal{L}_{\alpha;[\tau_L,\tau_U]}$

(i) The detection rates satisfy:

$$\mathcal{E}_D\left(\mathcal{L}_{\alpha;\hat{S}}\right) > \left[\mathcal{E}_D\left(\mathcal{L}_{\alpha;[\tau_L,\tau_U]}\right) + \left(\boldsymbol{\mathcal{M}}(\boldsymbol{\mathcal{A}}, \epsilon_{\alpha;D_A}) - 1\right)\right] \times \delta(\epsilon_{\alpha;D_A}, n_\alpha)$$

where $\epsilon_{\alpha;D_A} = \max_{a_1, a_2 \in \boldsymbol{\mathcal{S}}_{\alpha;\tau_U}} d(a_1, a_2)$.

(ii) The false alarm rates satisfy:

$$\mathcal{E}_F\left(\mathcal{L}_{\alpha;\hat{S}}\right) < \left[\mathcal{E}_F\left(\mathcal{L}_{\alpha;[\tau_L,\tau_U]}\right) - \left(\boldsymbol{\mathcal{M}}(\boldsymbol{\mathcal{A}}, \epsilon_{\alpha;F_A}) - 1\right)\right] \times \delta(\epsilon_{\alpha;F_A}, n_\alpha)$$

where $\epsilon_{\alpha;F_A} = \max_{a_1, a_2 \in \boldsymbol{\mathcal{S}}_{\alpha;\tau_L}} d(a_1, a_2)$.

Proof: The proof outline is similar for both Parts (i) and (ii). We compute a cell $\boldsymbol{\mathcal{C}}_\tau$ for $\mathcal{L}_{\alpha;[\tau_L,\tau_U]}$ on the state space $\boldsymbol{\mathcal{A}}$,

in which $\mathcal{L}_{\alpha;[\tau_L,\tau_U]}$ does not make an error and calculate its diameter to derive the underlying ϵ_A values, $\epsilon_{\alpha;D_A}$ for detection rate and $\epsilon_{\alpha;F_A}$ for false alarm rate, of the localization algorithm. Then, we utilize the ϵ_A value, computed from these diameters, for $\mathcal{L}_{\alpha;\hat{S}}$ and exploit the monotonicity of $\delta(\cdot)$ in n and N to ensure that $\hat{A}_S$ is within the ϵ_A-precision region. Lastly, we compute the ϵ_A-packing of the state space and identify the cell corresponding to $\boldsymbol{\mathcal{C}}_\tau$ in which $\mathcal{L}_{\alpha;[\tau_L,\tau_U]}$ makes a correct decision. In all the other cells $\mathcal{L}_{\alpha;\hat{S}}$ does not make an error with probability δ and hence it offers better performance than the former.

We now detail the bounds on the detection rate in Part (i), which assumes that the source is present. Let $\boldsymbol{S}_{\tau_U}$ denote the centroid of $\boldsymbol{\mathcal{S}}_{\tau_U}$ and let $\boldsymbol{\mathcal{C}}_{\tau_U}$ denote the cell of radius ϵ_{D_A} centered at $\boldsymbol{S}_{\tau_U}$. Consider a ϵ_{D_A}-packing of the state space (translated if needed) such that one of its cells aligns exactly with $\boldsymbol{\mathcal{C}}_{\tau_U}$. For fixed τ_L and τ_U, $\mathcal{L}_{\tau_L,\tau_U}$ does not make an error if the source lies inside $\boldsymbol{\mathcal{C}}_{\tau_U}$ – more precisely, if the source intensity $A_S \in \{a | a \in \boldsymbol{\mathcal{C}}_{\tau_U}\}$. But $\boldsymbol{\mathcal{S}}_{\tau_U}$ will make an error everywhere else, in particular on all the other cells of the ϵ_A-packing of the state space. There are $\boldsymbol{\mathcal{M}}(\boldsymbol{\mathcal{A}}, \epsilon_{D_A})$ cells inside the state space. Only one such cell corresponds to $\boldsymbol{\mathcal{C}}_{\tau_U}$ over which the detection does not make an error. On the other hand, $\boldsymbol{\mathcal{L}}_{\hat{S}}$ does not make an error on any of the cells, but with probability δ. Thus, the detection probability of $\mathcal{L}_{\alpha;\hat{S}}$ corresponding to these cells is at least $[(\boldsymbol{\mathcal{M}}(\boldsymbol{\mathcal{A}}, \epsilon_{D_A}) - 1)]\,\delta(\epsilon_{D_A}, n)$. For the cell $\boldsymbol{\mathcal{C}}_{\tau_U}$, however, detection by $\mathcal{L}_{\alpha;[\tau_L,\tau_U]}$ is with probability 1 and that by $\mathcal{L}_{\alpha;\hat{S}}$ is with probability δ, which leads to the inequality in Part (i). □

The implications of the above theorem are qualitatively similar to those in the next section derived for measurements from different sensor locations, and we will describe the two cases together.

B. Network Measurements

From measurements collected at different sensor locations, the localization-based SPRT $\mathcal{L}_{\mathbf{w};\hat{S}}$ is obtained as follows. Based on the source-present and background intensity estimates $\hat{A}_S$ and $\hat{B}$ obtained from the localization algorithm, we estimate $\hat{\mathbf{A}} = [\hat{A}_1 \hat{A}_2 \ldots \hat{A}_N]$ and $\hat{\mathbf{B}} = [\hat{B}_1 \hat{B}_2 \ldots \hat{B}_N]$, where $\hat{A}_i = F_S(\hat{A}_S, x_S, y_S, x_i, y_i)$ as defined in a previous section and $\hat{B}_i = \hat{B}$ for all i. Furthermore, the measurement weights are:

$$\hat{w}_i = \frac{\hat{A}_i + \hat{B}_i}{\hat{A}_i}.$$

We utilize these quantities to compute the threshold functions of $\mathcal{L}_{\mathbf{w};\hat{S}}$ as follow:

$$\begin{aligned} F_L(P_{0,1}, P_{1,0}, \hat{\mathbf{A}}, \hat{\mathbf{B}}, N) &< \sum_{i=1}^{N} \hat{w}_i m_i \\ &< F_U(P_{0,1}, P_{1,0}, \hat{\mathbf{A}}, \hat{\mathbf{B}}, N) \end{aligned}$$

The localization-based weighted-SPRT $\mathcal{L}_{\mathbf{w};\hat{S}}$ requires the measurements from all the sensors, which are used by its component localization algorithm to estimate $\hat{A}_S$.

Let A_i and B_i be the source intensity and background levels, respectively, at the sensor that collected measurement m_i. For $\alpha = \mathbf{w}$, we consider generalizations of the upper-threshold and lower-threshold sets defined in the previous section as follows:

$$\begin{aligned} \boldsymbol{\mathcal{S}}_{\mathbf{w};\tau_L} = \{A_S \in \boldsymbol{\mathcal{A}} &\mid \tau_L = F_L(P_{0,1}, P_{1,0}, \mathbf{A}, \mathbf{B}, N); \\ &A_i \geq w_i F_S(A_S, x_S, y_S)\}, \quad \text{and} \\ \boldsymbol{\mathcal{S}}_{\mathbf{w};\tau_U} = \{A_S \in \boldsymbol{\mathcal{A}} &\mid \tau_L = F_U(P_{0,1}, P_{1,0}, \mathbf{A}, \mathbf{B}, N); \\ &A_i \geq w_i F_S(A_S, x_S, y_S)\}. \end{aligned}$$

For the case of sensor measurements collected at different sensor locations, we have the following version of Theorem 5.1, which can be proved in a similar way.

Theorem 5.2: Consider the detection of a source using weighted-separable SPRTs. For SPRT $\mathcal{L}_{\mathbf{w};\hat{S}}$, based on a monotone δ-robust localization method and any threshold-based SPRT $\mathcal{L}_{\mathbf{w};[\tau_L,\tau_U]}$ for sufficiently large $n_{\mathbf{w}} = n$.

(i) The detection rates satisfy:

$$\begin{aligned} &\mathcal{E}_D\left(\mathcal{L}_{\mathbf{w};\hat{S}}\right) > \\ &\left[\mathcal{E}_D\left(\mathcal{L}_{\mathbf{w};[\tau_L,\tau_U]}\right) + (\boldsymbol{\mathcal{M}}(\boldsymbol{\mathcal{A}}, \epsilon_{\mathbf{w};D_A}) - 1)\right] \\ &\qquad \times \delta(\epsilon_{\alpha;D_A}, n_{\mathbf{w}}, N) \end{aligned}$$

where $\epsilon_{\mathbf{w};D_A} = \max_{a_1,a_2 \in \boldsymbol{\mathcal{S}}_{\mathbf{w};\tau_U}} d(a_1, a_2)$;

(ii) The false alarm rates satisfy:

$$\begin{aligned} &\mathcal{E}_F\left(\mathcal{L}_{\mathbf{w};\hat{S}}\right) < \\ &\left[\mathcal{E}_F\left(\mathcal{L}_{\mathbf{w};[\tau_L,\tau_U]}\right) - (\boldsymbol{\mathcal{M}}(\boldsymbol{\mathcal{A}}, \epsilon_{\mathbf{w};F_A}) - 1)\right] \\ &\qquad \times \delta(\epsilon_{\mathbf{w};F_Z}, n_{\mathbf{w}}, N) \end{aligned}$$

where $\epsilon_{\mathbf{w};F_A} = \max_{a_1,a_2 \in \boldsymbol{\mathcal{S}}_{\mathbf{w};\tau_L}} d(a_1, a_2)$.

The overall implications of Theorems 5.1 and 5.2 are quite similar, and we now summarize both by using the index $\alpha = 1, 2, \ldots, N, \mathbf{w}$ to cover both cases. The performance of $\mathcal{L}_{\alpha;\hat{S}}$ in terms of both expected detection and false alarm $\mathcal{E}_D$ and $\mathcal{E}_F$, is better than that of $\mathcal{L}_{\alpha;[\tau_L,\tau_U]}$ by a factor proportional to the packing number $\boldsymbol{\mathcal{M}}(\cdot)$ and $\delta(\cdot)$ with appropriate parameters. Qualitatively speaking, a "larger" state space will have a larger packing number, and hence $\mathcal{L}_{\alpha;\hat{S}}$ will lead to more effective detection. In particular, the performance of $\mathcal{L}_{\alpha;\hat{S}}$ will be increasingly better as one considers a larger intensity space $\mathcal{A}$, more sensors N, and more measurements n_α. The performance comparisons in Theorems 5.1 and 5.2 are valid no matter how the thresholds are chosen for $\mathcal{L}_{\alpha;[\tau_L,\tau_U]}$; for example, they can be based on domain-specific knowledge as in radiation source detection, Bayesian inference, or Dempster-Shafer theory.

VI. Conclusion

We formulated the facility activity inference problem with known location but unknown intensity using random sensor measurements in presence of a background process. We devised one-sided intensity-estimation SPRTs and discussed experimental results and performance comparisons based on IRSS and HFIR datasets. We then presented analytical results that establish performance bounds on detection and false alarm rates of the network detection method relative to single sensors

and simple majority approaches. Moreover, we analytically established the superior detection performance of the network over individual sensors with fixed and adaptive thresholds.

Our results lead to the following conclusions: (i) These LH-IE SPRTs are effective in inferring the on/off status of a reactor facility. However, the best results require fusing all sensors within a set radius from the facility. (ii) Overall, the fusion of multiple sensors provides better performance compared to those based on individual sensors. (iii) LH-IE SPRT fuser outperforms the simple majority LH-IE SPRT, thereby illustrating the importance of the fuser choice.

Future work may result in further improvements to our method. A consistently effective way of establishing an admissible sensor distance from the source should be devised. Similarly, defining an optimal window size is yet to be determined, since from our experimental results we can conclude that increasing the size almost monotonically improves or worsens the results. It would be of interest to investigate the number of window measurements needed by the network LH-IE SPRT to reach an optimal decision. Additional future work includes further simulations and datasets experimentation, and integration of other sensor modalities such as acoustic, biota, power supplies and cooling towers.

REFERENCES

[1] G. F. Knoll, *Radiation Detection and Measurement*. John Wiley, 2000.

[2] P. K. Varshney, *Distributed Detection and Data Fusion*. Springer-Verlag, 1997.

[3] S. M. Brennan, A. M. Mielke, and D. C. Torney, "Radiation detection with distributed sensor networks," *IEEE Computer*, pp. 57–59, August 2004.

[4] A. Sundaresan, P. K. Varshney, and N. S. V. Rao, "Distributed detection of a nuclear radiaoactive source using fusion of correlated decisions," in *International Conference on Information Fusion*, 2007.

[5] N. S. V. Rao, S. Sen, N. J. Prins, D. A. Cooper, R. J. Ledoux, J. B. Costales, K. Kamieniecki, S. E. Korbly, J. K. Thompson, J. Batcheler, R. R. Brooks, and C. Q. Wu, "Network algorithms for detection of radiation sources," *Nuclear Instruments and Methods Phy. Res. A*, vol. 784, pp. 326–331, Jun. 2015.

[6] P. E. Felau, "Comparing a recursive digital filter with the moving-average and sequential probability-ratio detection methods for SNM portal monitors," *IEEE Transactions on Nuclear Science*, vol. 40, no. 2, pp. 143–146, 1993.

[7] K. D. Jarman, L. E. Smith, and D. K. Carlson, "Sequential probability ratio test for long-term radiation monitoring," *IEEE Transactions on Nuclear Science*, vol. 51, no. 4, pp. 1662–1666, 2004.

[8] K. E. Nelson, J. D. Valentine, and B. R. Beauchamp, "Radiation detection method and system using the sequential probability ratio test," 2007, u.S. Patent 7,244,930 B2.

[9] N. S. V. Rao, C. Y. T. Ma, and D. K. Y. Yau, "On performance of individual, collective and network detection of propagative sources," in *International Conference on Information Fusion*, 2013.

[10] N. S. V. Rao, M. Shankar, J. C. Chin, D. K. Y. Yau, Y. Yang, X. Xu, and S. Sahni, "Improved SPRT detection using localization with application to radiation sources," in *International Conference on Information Fusion*, 2009.

[11] N. S. V. Rao, S. Sen, M. L. Berry, C. Q. Wu, K. M. Grieme, R. R. Brooks, and G. Cordone, "Datasets for radiation network algorithm development and testing," in *2016 IEEE Nuclear Science Symposium*, 2016.

[12] "Canonical irss datasets." [Online]. Available: https://github.com/raonsv/canonical-datasets

[13] D. E. Archer, B. R. Beauchamp, J. G. Mauger, K. E. Nelson, M. B. Mercer, D. C. Pletcher, V. J. Riot, J. L. Schek, and D. A. Knapp, "Adaptable radiation monitoring system and method," 2006, u.S. Patent 7,064,336 B2.

[14] N. L. Johnson, "Sequential analysis: A survey," *Journal of Royal Statistical Society, Series A*, vol. 124, no. 3, pp. 372–411, 1961.

[15] J. C. Chin, N. S. V. Rao, D. K. Y. Yau, M. Shankar, S. Srivathsan, S. S. Iyengar, Y. Yang, and J. C. Hou, "Identification of low-level point radioactive sources using a sensor network," *ACM Transactions on Sensor Networks*, 2010.

[16] L. Devroye, L. Gyorfi, and G. Lugosi, *A Probabilistic Theory of Pattern Recognition*. Springer-Verlag, New York, 1996.

[17] N. S. V. Rao, J. C. Chin, D. K. Y. Yau, and C. Y. T. Ma, "Localization leads to improved distribution detection under non-smooth distributions," in *International Conference on Information Fusion*, 2010.